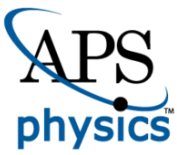

Synchronous Spin-Exchange Optical Pumping

A. Korver, D. Thrasher, M. Bulatowicz, and T. G. Walker

Phys. Rev. Lett. **115**, 253001 — Published 18 December 2015

DOI: 10.1103/PhysRevLett.115.253001

Synchronous Spin-Exchange Optical Pumping

A. Korver, D. Thrasher, M. Bulatowicz, and T. G. Walker
Department of Physics, University of Wisconsin-Madison, Madison, WI 53706, USA
(Dated: November 18, 2015)

We demonstrate a new approach to precision NMR with hyperpolarized gases designed to mitigate NMR shifts due to the alkali spin-exchange field. The NMR bias field is implemented as a sequence of alkali (Rb) 2π pulses, allowing the Rb polarization to be optically pumped transverse to the bias field. When the Rb polarization is modulated at the noble-gas (Xe) NMR resonance, spin-exchange collisions build-up a precessing transverse Xe polarization. We study and mitigate novel NMR broadening effects due to the oscillating spin-exchange field. Spin-exchange frequency shifts are suppressed $2500\times$, and Rb magnetometer gain measurements project photon shot-noise limited NMR frequency uncertainties below 10 nHz/$\sqrt{\text{Hz}}$.

The ability to produce highly magnetized noble gases via spin-exchange collisions with spin-polarized alkali atoms [1] has greatly impacted scientific studies of magnetic resonance imaging [2], high-energy nuclear physics with spin-polarized targets [3], and chemical physics [4]. Applications in precision measurements began with NMR gyros [5] and have continued with fundamental symmetry tests using multiple cell free induction decay [6], dual-species masers [7, 8], self-compensating co-magnetometers [9], NMR oscillators [10], and free spin-precession co-magnetometers [11–14].

Some of these approaches [5, 9–11, 14] take advantage of enhanced NMR detection by the embedded alkali magnetometer. The alkali and noble-gas spin ensembles experience enhanced polarization sensitivity due to the Fermi-contact interaction during collisions between the two species. The two species experience effective Fermi-contact fields

$$\boldsymbol{B}_{SK} = b_{SK}\langle \boldsymbol{K}\rangle = \frac{8\pi\kappa}{3}\frac{\mu_K}{K} n_K \langle \boldsymbol{K}\rangle \tag{1}$$

$$\text{and } \boldsymbol{B}_{KS} = b_{KS}\langle \boldsymbol{S}\rangle = -\frac{8\pi\kappa}{3} g_S \mu_B n_S \langle \boldsymbol{S}\rangle, \tag{2}$$

where $\boldsymbol{S}, \boldsymbol{K}$ are the electron and nuclear spin operators, n_S, n_K the atomic densities, μ_K the nuclear magnetic moment of the noble gas, μ_B the Bohr magneton, and the atomic g-factor $g \approx 2$. The frequency-shift enhancement factor κ [15, 16] was recently measured to be 493 ± 31 [17] for RbXe. Thus the detected NMR field $\boldsymbol{B}_{SK}$ is $\sim 500\times$ larger for the embedded magnetometer than for any external sensor. This seemingly decisive advantage comes with the cost of similarly enhancing the $\boldsymbol{B}_{KS}$ field due to the spin-polarized Rb atoms, 190 μG at $2n_S\langle \boldsymbol{S}\rangle = 10^{13}$ cm^{-3}. In typical longitudinally polarized NMR this field produces large frequency shifts of order 0.1 Hz. One approach for mitigating this effect is to compare two Xe isotopes [5, 11], for which the enhancement factors are equal to about 0.2% [11]. Another recent strategy nulls the alkali field by saturating the alkali electron spin resonance during free precession intervals [14].

This Letter describes a new approach, synchronous spin-exchange optical pumping, in which both the alkali (here, Rb) and noble gas spins (Xe) are polarized transverse to the bias magnetic field. See Fig. 1. The bias magnetic field is applied as a sequence of short Rb 2π pulses, allowing the Rb atoms to be polarized perpendicular to the bias field [18]. By

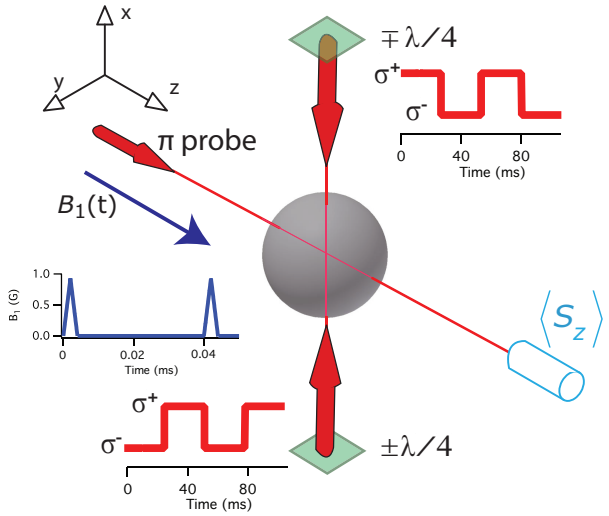

FIG. 1. Essential components of synchronous spin-exchange optical pumping. An NMR bias field $\boldsymbol{B}_1(t)$ is applied as a sequence of short alkali 2π pulses, allowing the atoms to be optically pumped with resonant light perpendicular to $\boldsymbol{B}_1$ with periodic polarization reversals from the polarization modulators. Spin-exchange collisions between Xe atoms and the oscillating Rb spins drive the NMR resonance. The field produced by the precessing Xe nuclei rotates the Rb spins, causing a Faraday rotation of the polarization of the probe light.

periodically reversing the Rb polarization direction at the Xe resonance frequency, transverse nuclear polarization is resonantly generated by spin-exchange collisions. On resonance, the Rb polarization is in phase with the noble-gas precession, so there is no time-averaged torque from the alkali field and therefore no frequency shift of the NMR resonance. However, when the Rb polarization is modulated off-resonance, we find that the torque from the alkali field suppresses the phase shift of the NMR precession and generates a longitudinal component of the Xe polarization. This results in a novel broadening of the NMR resonance that is readily suppressed by adding an AC compensation field 180° out of phase with and along the same direction as the Rb polarization modulation. So compensated, this approach thus maintains the SNR advantages of NMR detection by the embedded alkali magnetometer, while suppressing the Fermi contact field broadening and shifts.

Synchronous spin-exchange is accomplished by a colli-

sional variant of the Bell-Bloom method of synchronous optical pumping [19]. The nuclei are polarized by spin-exchange collisions with alkali-metal atoms whose spin, oriented transverse to a bias magnetic field $\boldsymbol{B}_1 = B_1(t)\hat{z}$, oscillates at the nuclear Larmor frequency. The combined effects of Larmor precession, transverse spin-relaxation, and spin-exchange collisions are described by the Bloch equation for the transverse spin components $\langle K_+\rangle = \langle K_x\rangle + i\langle K_y\rangle$:

$$\frac{d\langle K_+\rangle}{dt} = -(i\gamma_K \bar{B}_1 + \Gamma_2)\langle K_+\rangle + \Gamma_{\rm SE}\langle S_x\rangle(t) \qquad (3)$$

The noble-gas gyromagnetic ratio is γ_K, the transverse relaxation rate of the nuclei is Γ_2, and the spin-exchange collision rate is $\Gamma_{\rm SE}$. A notable omission from Eq. 3 is the torque from the magnetic field $\hat{x}b_{KS}\langle S_x\rangle(t)$ produced by the alkali spins, which we temporarily assume has been eliminated as will be explained in detail below.

The alkali spin-polarization $\langle S_x\rangle(t) = \sum_q s_q e^{-iq\omega t}$ is modulated by the pumping light at a frequency ω near the p-th submultiple of the time-averaged noble-gas resonance frequency $\omega_0 = \gamma_K \bar{B}_1$. In the rotating-wave approximation we neglect all but the near-resonant co-rotating Fourier component s_p, which produces a transverse noble-gas polarization

$$\langle K_+\rangle = \frac{\Gamma_{\rm SE} s_p e^{-ip\omega t}}{\Gamma_2 + i(\omega_0 - p\omega)} = \langle \tilde{K}_+\rangle e^{-ip\omega t} \qquad (4)$$

with the usual amplitude and phase response of a driven oscillator. On resonance, the transverse polarization in the rotating frame, $\langle \tilde{K}_+\rangle$, has a magnitude $K_{\max} = \Gamma_{\rm SE} s_p/\Gamma_2$. Off-resonance, the rotating frame magnetic field $\hat{z}(\omega_0 - p\omega)/\gamma_K$ causes the polarization to tilt in the x-y plane by an angle $\delta\phi = \tan^{-1}[(\omega_0 - p\omega)/\Gamma_2]$. In comparison to the usual longitudinal spin-exchange [1], the maximum polarization attainable depends on a competition between $\Gamma_{\rm SE}$ and Γ_2 rather than the longitudinal relaxation rate Γ_1. The polarization is also reduced by the Fourier amplitude $|s_p|/|\langle S_x\rangle| \approx 2/\pi p$ for our roughly square wave polarization modulation. When combined with a feedback system to actively null the phase shift $\delta\phi$, the resonance frequency is an accurate measure of the Larmor frequency: $\omega = \omega_0/p$. Thus synchronous spin-exchange is attractive for accurate absolute magnetometry and rotation sensing.

The synchronously oscillating transverse alkali polarization, an impossibility in a DC magnetic field due to the ~ 1000 fold larger magnetic moment as compared to Xe, is enabled by replacing the usual DC bias field by $B_1(t)$, a sequence of short (4 μs) pulses. Each pulse produces 2π precession of the alkali atoms [18], *i.e.* $\int \gamma_{Rb} B_1 dt = 2\pi$. Here the Rb gyromagnetic ratio is $\gamma_{Rb} = \gamma_S/(2I+1) \approx \mu_B/3\hbar$ for the ^{85}Rb isotope we use. The application of a sequence of 2π pulses causes no time-averaged precession of the Rb spins, thereby allowing the Rb to be optically pumped as if in zero field. Meanwhile, the polarized Xe nuclei precess only $2\pi\gamma_{Xe}/\gamma_{Rb} \approx 5$ mrad per pulse (for ^{131}Xe) and effectively sense only the DC average $\bar{B}_1$.

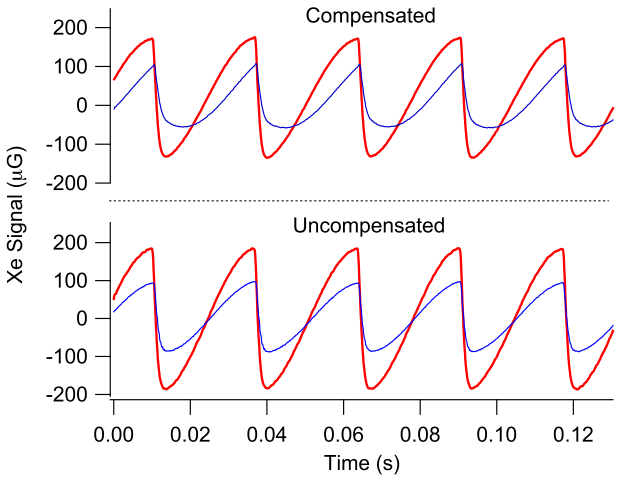

FIG. 2. Xe precession signals detected by the embedded Rb magnetometer. The magnetometer gain reversals square-wave modulate the sinusoidal Xe precession. When the Rb spin-exchange field is compensated, signals detuned by one half-linewidth (blue) are smaller in amplitude and phase-shifted with respect to the on-resonance case (red). Uncompensated, the spin-exchange fields greatly suppress phase shifts.

The apparatus includes a nominally spherical 8 mm diameter glass cell that contains Rb vapor (density $0.2 - 3 \times 10^{13}$ cm^{-3}), 32 Torr of ^{131}Xe, 4 Torr of ^{129}Xe, and 300 Torr of N_2. The cell is held inside a ceramic oven that is heated by running 20 kHz AC current through commercial Kapton flex-circuit heater strips that are configured to minimize stray fields. Outside the oven are Helmholtz field coils for fine-shimming of the 3 magnetic field components, plus a set of 4 coils for generating the 2π pulses. The oven and coils are inside a 3 layer magnetic shield with optical access ports for the lasers. The 2π coils are designed to maximize uniformity, maintain low inductance, and minimize stray fields that couple to the shields. They are driven by a custom MOSFET circuit designed to minimize pulse-to-pulse charge fluctuations.

Optical pumping is performed using two free-running 40 mW 795 nm distributed feedback diode lasers that are combined on a non-polarizing beamsplitter. One of the lasers is tuned above the Rb D1 resonance, the other below. Since the AC Stark field changes sign at resonance, we can reduce the effective field from about 2 mG (for a single pumping frequency) to < 10 μG by adjusting the relative detunings and intensities of the two lasers. The two output beams from the polarizing beamsplitter, each containing both pump frequencies, enter the cell and propagate along along the $\pm\hat{x}$ directions; doing this substantially improves the uniformity of the optical pumping of the optically thick alkali vapor. The last optical elements before the cell are wave plates and liquid crystal variable retarders that allow the circular light polarizations to be reversed in about 200 μs. At low Rb density, the laser detunings are selected to produce about 70% Rb polarization while nulling the AC Stark shifts. At high densities the

polarization drops to about 40% without significantly degrading the AC Stark cancellation.

An off-resonant 6 mW probe laser, propagating along $\hat{z}$, serves to observe the z-component of the alkali polarization using low-noise Faraday rotation detection. Because the alkali atoms are optically pumped along $\hat{x}$, the Faraday rotation detects the $\hat{y}$-component of the Xe field: $\langle S_z\rangle = -\gamma_S b_{SK}\langle K_y\rangle\langle S\rangle_x(t)/\Gamma'$. Note that the magnetometer sensitivity reverses sign as the alkali spin direction is reversed due to the synchronous pumping. In order to detect $\langle K_z\rangle$, we add a $\boldsymbol{B}_2$ =1 mG $\hat{x}\sin(\omega_2 t)$ field at $\omega_2 = 900$ Hz [20]. Demodulation of $\langle S_z\rangle$ at ω_2 then gives an output approximately equal to $-\gamma_S B_2 b_{SK}\langle K_z\rangle\langle S\rangle_x(t)/\Gamma'^2$. Characterization of the magnetic response implies a relaxation rate $\Gamma' = 120000$/s with a magnetic response bandwidth of 1.5 kHz and a dynamic range of 5.7 mG. The noise floor of the magnetometer is typically a few nG/$\sqrt{\text{Hz}}$.

To null stray DC magnetic fields, we temporarily turn off the 2π pulses while retaining the pump modulation, effectively running the magnetometer as a zero-field magnetometer with polarization modulation. After field nulling with the zero-field magnetometer, we turn on the 2π pulses. The area of the 2π pulses is set to better than 0.1% by nulling the magnetometer signal generated by $\boldsymbol{B}_2$. The 25 kHz repetition rate of the 2π pulse sequence and the modulation waveform for the optical pumping are generated by direct digital synthesis using an FPGA phase-locked to a commercial atomic Rb clock. With stray fields nulled and the 2π pulse area set, the synchronously pumped Xe signals are readily observed when the pumping modulation frequency ω is brought near either the $\omega_0 = 2\pi \times 18.702$ Hz ^{131}Xe resonance frequency or the $\omega_0 = 2\pi \times 21.03$ Hz 3rd subharmonic of the ^{129}Xe resonance frequency. A magnetometer waveform is shown in Fig. 2, and a sample spin-exchange resonance curve is shown in Fig. 3b. The resonance curve is taken by lock-in detection of the 2ω magnetometer signal. The in-phase lock-in output is proportional to $\tilde{K}_x$ while the quadrature is proportional to $\tilde{K}_y$. The $p = 1$ signal amplitude, typically 180 μG for both isotopes at $n_S = 2.5 \times 10^{13}$ cm^{-3}, is consistent with expectations from independent measurements of Γ_1, $\Gamma_{\rm SE}$, and S_x.

So far we have ignored possible effects from the alkali field; indeed the resonance in Fig. 3b was taken with a compensated alkali field as will be explained below. However, when uncompensated the alkali field can have a dramatic effect. Under the conditions of Fig. 3a, the in-phase response is broadened by a factor of 4 as compared to Fig. 3b. Even more dramatic is the observed suppression of the quadrature signal by 10x, while a dispersive z-polarization is acquired. At higher densities we have observed broadening of up to 10$\times$ and quadrature suppression of 75$\times$ for ^{129}Xe.

The broadening from the spin-exchange field can be understood as follows. First, when the pumping is off-resonance, the phase shift $\delta\phi$ between the nuclear precession and the alkali field produces a DC torque $-\gamma_K \boldsymbol{B}_{KS} \times \langle \boldsymbol{K}\rangle = \frac{2}{p\pi}\gamma_K |B_{KS}| K_\perp \sin\delta\phi$ and so the Xe spin develops a z-polarization. The z-polarization, which can be a substantial fraction of the transverse polarization (as illustrated in Fig. 3a), then couples with the alkali field to produce a transverse torque that is 90 degrees out of phase with the pumping. This can be considered as a negative feedback mechanism that tries to null the relative phase between the Xe precession and the pumping. The net effect is to generate a large z-polarization and to suppress the phase shift between the pumping and the Xe precession. Under our conditions the alkali field, when uncompensated, is sufficiently strong to make $|\langle K_z\rangle| > |\langle K_x\rangle|$ at large detunings.

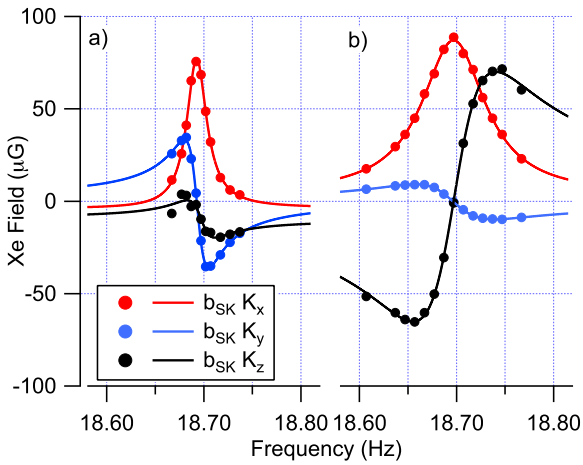

FIG. 3. NMR line shapes for synchronously pumped ^{131}Xe, $n_S = 7.1 \times 10^{12}$ cm^{-3}. Left: when the spin-exchange field is compensated, the rotating-frame polarizations show the expected Lorentzian forms (red: in phase or $\tilde{K}_x$, blue: $\tilde{K}_y$, black: K_z), and little longitudinal polarization is generated. Right: An uncompensated spin-exchange field not only broadens the NMR resonance, but produces large z-polarizations and dramatically suppresses the rotating frame quadrature component.

The Bloch equation for the z-polarization is

$$\frac{d\langle K_z\rangle}{dt} = -\gamma_K b_x(t)\langle K_y\rangle - \Gamma_1\langle K_z\rangle \tag{5}$$

which leads to a steady-state

$$\langle K_z\rangle = \frac{\gamma_K b_{xp}}{\Gamma_1} K_\perp \sin(\delta\phi) = \tan(\alpha) K_\perp \sin(\delta\phi) \tag{6}$$

The effective magnetic field $b_x(t)$ seen by the Xe nuclei is the sum of the alkali field and an anti-parallel square-wave modulated external compensation field: $b_x(t) = b_{KS}\langle S_x\rangle(t) - B_c(t)$. The p-th Fourier component of this field is b_{xp}. Both the spin-exchange field and the compensation field are slightly phase-shifted with respect to the light polarization reversals due to the finite optical pumping time, visible in Fig. 2. The size of the spin-exchange torque is characterized by the parameter $\tan(\alpha) = \gamma_K b_{xp}/\Gamma_1$.

The z-polarization of the Xe now allows the transverse fields to apply a torque, so the transverse components of the Bloch equations become

$$\frac{d\langle K_+\rangle}{dt} = -(i\gamma_K \bar{B}_1 + \Gamma_2)\langle K_+\rangle + i\gamma_K b_x\langle K_z\rangle + \Gamma_{\rm SE}\langle S_x\rangle$$

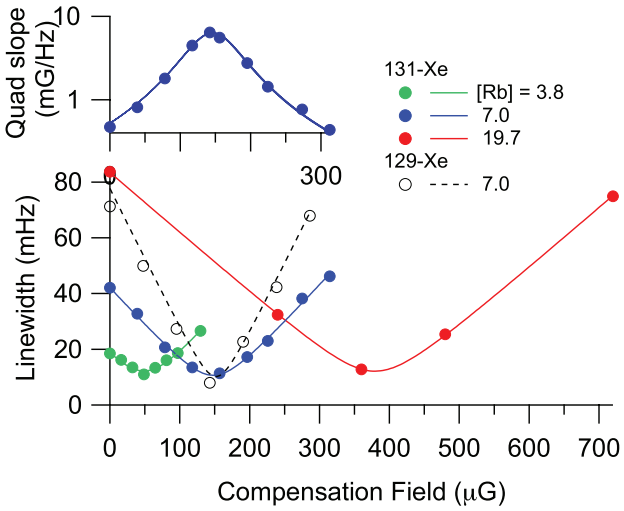

FIG. 4. Comparison of observed spin-exchange broadening with Eqs. 8 and 10. (bottom) The broadening of the NMR linewidth due to the spin-exchange field can be eliminated by applying a compensation field that oscillates 180° out of phase with the spin-exchange field. Solid lines and dots show ^{131}Xe linewidths, dashes and unfilled dots show a sample for ^{129}Xe. Densities are listed in units of 10^{12} cm^{-3}. (top) Representative measurement of the slope of the quadrature signal as a function of compensation field.

$$\approx -(i\gamma_K \bar{B}_1 + \Gamma_2)\langle K_+\rangle + \left(i\Gamma_1 \tan^2(\alpha)\sin(\delta\phi)K_\perp + \Gamma_{\rm SE}s_p\right)e^{-ip\omega t} \quad (7)$$

where we have again made the rotating wave approximation. Notice that the torque from the alkali field is 90° out of phase with the pumping torque, acting to suppress the phase shift between the pumping and the precession. The steady-state polarization in the rotating frame is

$$\langle \tilde{K}_+\rangle = \frac{K_{\rm max}}{1+\Delta^2/\Gamma_{\rm eff}^2}\left(1 + i\frac{\Gamma_2\Delta}{\Gamma_{\rm eff}^2}\right) \quad (8)$$

$$\langle K_z\rangle = -\langle \tilde{K}_y\rangle \tan\alpha \quad (9)$$

where the spin-exchange broadened linewidth is

$$\Gamma_{\rm eff} = \sqrt{\Gamma_2^2 + \Gamma_1\Gamma_2\tan^2\alpha} = \sqrt{\Gamma_2^2 + \frac{\Gamma_2}{\Gamma_1}(\gamma_K b_{xp})^2} \quad (10)$$

and the detuning is $\Delta = p\omega - \omega_0$. For a large spin-exchange field, $\tan\alpha \gg 1$, these equations account for the observed broadening, small $\left\langle \tilde{K}_y \right\rangle$ response, and large $\langle K_z\rangle$ response. They also predict that with the application of a compensation field B_c 180° out of phase with the pumping, the linewidth narrows to Γ_2, the magnitude of $\left\langle \tilde{K}_y \right\rangle$ is restored, and $\langle K_z\rangle$ is suppressed, thus bringing the response into agreement with Eq. 4. All these features are illustrated in the data of Fig. 3, with fits to Eqs 8-10. The line-width formula (10) is reminiscent of power broadening [21], but spin-exchange broadening does not reduce the on-resonant signal size.

We have studied the spin-exchange broadening over a range of alkali field strengths for both Xe isotopes. Figure 4 shows the predicted narrowing of the resonance width with application of the compensation field. For Xe-129 there is an order of magnitude narrowing of the width over the field range, despite having reduced $\tan(\alpha)$ by a factor of 3 by pumping at the third subharmonic of the Larmor frequency. We have confirmed that at a given density the compensation fields for ^{129}Xe and ^{131}Xe are the same to within 1%. Figure 4 also shows an example of how the quadrature slope $d\tilde{K}_y/d\Delta$ dramatically increases as the compensation field approaches the optimum. We have observed as much as a factor of 75 ratio between the compensated and uncompensated slopes.

At higher densities than reported in this paper, the broadening slows as a function of compensation field. We believe that this arises because of feedback from the alkali field: at sufficiently high densities, the tipping of the alkali field off of the $\hat{x}$-axis becomes important and needs to be taken into account. Such non-linearities are likely closely related to the studies of strongly coupled alkali and noble gas spin from Ref. [22].

We can estimate the degree to which synchronous spin-exchange eliminates the alkali field by measuring the DC value of $\langle S_z\rangle$, which produces a frequency shift $b_{KS}\langle S_z\rangle$. At a Rb density of 2.3×10^{13} cm^{-3} we find $\langle S_z\rangle < 2\times10^{-4}$, equivalent to an alkali field of 170 nG which is a factor of 2500 reduction as compared to longitudinally polarized NMR.

In the future, two-species operation will allow full realization of the spectroscopy potential of synchronous spin-exchange for fundamental symmetry tests. With two-species, one can be used to remove magnetic field noise, leaving the other sensitive to non-magnetic interactions. In a dual Xe isotope implementation, the residual alkali field of 170 nG would produce a differential frequency shift of 240 nHz, with an expected stability substantially better than that. Such strategies are used in many experiments [5, 7, 8, 11–14]. The effective frequency noise δx resulting from some non-magnetic interaction $H = hx$ is of order

$$\delta x = \left(1 + \frac{\gamma_2^2}{\gamma_1^2}\right)^{1/2}\frac{\Gamma_2\delta B}{2\pi b_{SK}K_\perp} \quad (11)$$

Our current apparatus is limited by probe technical noise at about the $\delta B = 2\times10^{-9}$ G/$\sqrt{\rm Hz}$ level, but even this relatively modest magnetometer performance projects to $\delta x = 110$ nHz/$\sqrt{\rm Hz}$. Supposing we can eliminate this technical noise and reach the photon shot noise limit of our Faraday detection, the projected NMR frequency noise level would be 7 nHz/$\sqrt{\rm Hz}$, competitive with the Ne-Rb-K co-magnetometer of Ref. [9]. These numbers are very promising for experiments such as sensitive tests of Lorentz violation [9] and limits on short-range nuclear interactions [11, 12].

Finally, synchronous spin-exchange promises not only sensitivity but accuracy. Configured as a dual-species oscillator [5] to actively null $\delta\phi$, for example, the nuclear phase becomes an accurate integral of the inertial rotation rate. The above noise estimates suggest an achievable rotation sensitivity approaching 100 μdeg/$\sqrt{\rm hr}$ for a synchronously pumped NMR gyro with a unity scale factor and a bandwidth that approaches the oscillation frequency.

We are grateful for many discussions with M. Larsen, R. Wyllie, B. Lancor, M. Ebert, and I. Sulai. This work was supported by NSF GOALI PHY1306880 and Northrop Grumman Corp.

[1] T. G. Walker and W. Happer, "Spin-exchange optical pumping of noble-gas nuclei," Rev. Mod. Phys. **69**, 629 (1997).

[2] Laura L. Walkup and Jason C. Woods, "Translational applications of hyperpolarized he-3 and xe-129," NMR Biomed. **27**, 1429–1438 (2014).

[3] Jaideep T. Singh, P. A. M. Dolph, W. A. Tobias, T. D. Averett, A. Kelleher, K. E. Mooney, V. V. Nelyubin, Yunxiao Wang, Yuan Zheng, and G. D. Cates, "Development of high-performance alkali-hybrid polarized ^{3}He targets for electron scattering," Phys. Rev. C **91**, 055205 (2015).

[4] Ricardo Jiménez-Martínez, Daniel J. Kennedy, Michael Rosenbluh, Elizabeth A. Donley, Svenja Knappe, Scott J. Seltzer, Hattie L. Ring, Vikram S. Bajaj, and John Kitching, "Optical hyperpolarization and nmr detection of 129xe on a microfluidic chip," Nat. Commun. **5** (2014).

[5] D. Meyer and M. Larsen, "Nuclear magnetic resonance gyro for inertial navigation," Gyroscopy and Navigation **5**, 75–82 (2014).

[6] T. G. Vold, F. J. Raab, B. Heckel, and E. N. Fortson, "Search for a permanent electric dipole moment on the ^{129}Xe atom," Phys. Rev. Lett. **52**, 2229–2232 (1984).

[7] Alexander G. Glenday, Claire E. Cramer, David F. Phillips, and Ronald L. Walsworth, "Limits on anomalous spin-spin couplings between neutrons," Phys. Rev. Lett. **101**, 261801 (2008).

[8] M. A. Rosenberry and T. E. Chupp, "Atomic electric dipole moment measurement using spin exchange pumped masers of ^{129}Xe and ^{3}He," Phys. Rev. Lett. **86**, 22–25 (2001).

[9] M. Smiciklas, J. M. Brown, L. W. Cheuk, S. J. Smullin, and M. V. Romalis, "New test of local lorentz invariance using a ^{21}Ne-Rb-**K** comagnetometer," Phys. Rev. Lett. **107**, 171604 (2011).

[10] A. Yoshimi, T. Inoue, T. Furukawa, T. Nanao, K. Suzuki, M. Chikamori, M. Tsuchiya, H. Hayashi, M. Uchida, N. Hatakeyama, S. Kagami, Y. Ichikawa, H. Miyatake, and K. Asahi, "Low-frequency 129xe nuclear spin oscillator with optical spin detection," Phys. Lett. A **376**, 1924 – 1929 (2012).

[11] M. Bulatowicz, R. Griffith, M. Larsen, J. Mirijanian, C. B. Fu, E. Smith, W. M. Snow, H. Yan, and T. G. Walker, "Laboratory Search for a Long-Range T-Odd, P-Odd Interaction from Axionlike Particles Using Dual-Species Nuclear Magnetic Resonance with Polarized Xe-129 and Xe-131 Gas," Phys. Rev, Lett. **111**, 102001 (2013).

[12] K. Tullney, F. Allmendinger, M. Burghoff, W. Heil, S. Karpuk, W. Kilian, S. Knappe-Grueneberg, W. Mueller, U. Schmidt, A. Schnabel, F. Seifert, Yu Sobolev, and L. Trahms, "Constraints on Spin-Dependent Short-Range Interaction between Nucleons," Phys Rev. Lett. **111**, 100801 (2013).

[13] F. Allmendinger, W. Heil, S. Karpuk, W. Kilian, A. Scharth, U. Schmidt, A. Schnabel, Yu. Sobolev, and K. Tullney, "New Limit on Lorentz-Invariance- and CPT-Violating Neutron Spin Interactions Using a Free-Spin-Precession He-3-Xe-129 Comagnetometer," Phys Rev. Lett. **112**, 110801 (2014).

[14] D. Sheng, A. Kabcenell, and M. V. Romalis, "New Classes of Systematic Effects in Gas Spin Comagnetometers," Phys Rev. Lett. **113**, 163002 (2014).

[15] B. C. Grover, "Noble-gas nmr detection through noble-gas-rubidium hyperfine contact interaction," Phys. Rev. Lett. **40**, 391 (1978).

[16] S. R. Schaefer, G. D. Cates, Ting-Ray Chien, D. Gonatas, W. Happer, and T. G. Walker, "Frequency shifts of the magnetic-resonance spectrum of mixtures of nuclear spin-polarized noble gases and vapors of spin-polarized alkali-metal atoms," Phys. Rev. A **39**, 5613–5623 (1989).

[17] Z. L. Ma, E. G. Sorte, and B. Saam, "Collisional ^{3}He and ^{129}Xe frequency shifts in rb˘noble-gas mixtures," Phys. Rev. Lett. **106**, 193005 (2011).

[18] A. Korver, R. Wyllie, B. Lancor, and T. G. Walker, "Suppression of spin-exchange relaxation using pulsed parametric resonance," Phys. Rev. Lett. **111**, 043002 (2013).

[19] William E. Bell and Arnold L. Bloom, "Optically driven spin precession," Phys. Rev. Lett. **6**, 280–281 (1961).

[20] Zhimin Li, Ronald T Wakai, and T.G. Walker, "Parametric modulation of an atomic magnetometer," Appl. Phys. Lett. **89**, 134105 (2006).

[21] A. Abragam, Principles of Magnetic Resonance (Springer-Verlag, New York, 1990).

[22] T. W. Kornack and M. V. Romalis, "Dynamics of two overlapping spin ensembles interacting by spin exchange," Phys. Rev. Lett. **89**, 253002 (2002).